Environmental Science & Technology Letters

Letter

Cite This: Environ. Sci. Technol. Lett. XXXX, XXX, XXX-XXX

pubs.acs.org/journal/estlcu

Fractal Dimensions and Mixing Structures of Soot Particles during Atmospheric Processing

Yuanyuan Wang,[†,‡] Fengshan Liu,[§] Cenlin He,[∥] Lei Bi,[‡] Tianhai Cheng,[⊥] Zhili Wang,[#] Hua Zhang,[@,▽] Xiaoye Zhang,[#] Zongbo Shi,[●] and Weijun Li*[,‡]

[†]Environment Research Institute, Shandong University, Jinan, Shandong 250100, China

[‡]Department of Atmospheric Sciences, School of Earth Sciences, Zhejiang University, Hangzhou 310027, China

[§]Measurement Science and Standards, National Research Council, Ottawa, Ontario K1A 0R6, Canada

[∥]Department of Atmospheric and Oceanic Sciences and Joint Institute for Earth System Science and Engineering, University of California, Los Angeles, California 90095, United States

[⊥]State Key Laboratory of Remote Sensing Science, Institute of Remote Sensing and Digital Earth, Chinese Academy of Sciences, Beijing 100101, China

[#]Chinese Academy of Meteorological Sciences, Beijing 100081, China

[@]Collaborative Innovation Center on Forecast and Evaluation of Meteorological Disasters, Nanjing University of Information Science & Technology, Nanjing 210044, China

[▽]Laboratory for Climate Studies, National Climate Center, China Meteorological Administration, Beijing 100081, China

[●]School of Geography, Earth and Environmental Sciences, University of Birmingham, Birmingham B15 2TT, U.K.

Supporting Information

ABSTRACT: Soot particles strongly absorb sunlight and hence act as a short-lived warming agent. Atmospheric aging of soot particles changes their morphology and mixing state and consequently alters their optical properties. Here we collected soot particles at tunnel, urban, mountaintop, and background sites in the North China Plain and analyzed their mixing structures and morphology using transmission electron microscopy. Soot particles were further classified into three types: bare-like, partly coated, and embedded. Bare-like soot particles were dominant at the tunnel site, while most soot particles were of the partly coated or embedded type at other sites. Fractal dimensions (D_f) of different types of soot particles ranged from 1.80 to 2.16 and increased in the following order: bare-like < partly coated < embedded. Moreover, their average D_f changed from 1.8 to 2.0 from the tunnel to the background site. We conclude that the D_f can characterize the shape of soot aggregates reasonably well, and its variation reflects soot aging processes. Compared with the reported D_f of soot particles, we found that the D_f value of 1.8 used in previous optical models primarily represents freshly emitted soot aggregates, rather than the ambient ones.

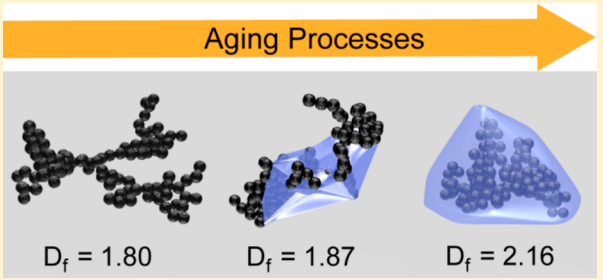

1. INTRODUCTION

Soot particles, also known as black carbon (BC) or elemental carbon (EC), are fractal-like aggregates produced from the incomplete combustion of biomass and fossil fuels. Soot particles strongly absorb sunlight and heat the air, altering the radiative forcing of the atmosphere and affecting the global climate and regional climates.[1−4] During transport and aging, fresh soot particles mix with organic and inorganic aerosols, which changes their morphology and compactness and further leads to variations in their optical properties and radiative forcing.[5,6] Jacobson[7] proposed that the sulfate coating on soot particles can enhance optical absorption by ∼2-fold via treatment of the mixture of soot and sulfate as a core−shell model. However, Cappa et al.[8] observed that the absorption enhancement of aged soot particles in Sacramento was 6% on average at 532 nm as determined by in situ measurements. Different conclusions about the optical absorption of soot particles should be attributed to their complicated shapes and various mixing states in the atmosphere.[9,10] Because of the lack of quantification on the variation of shapes and mixing structures of soot particles, the debate about the optical properties of soot particles continues.

Some experimental methods using a combination of a single-particle soot photometer (SP2), a three-wavelength photo-acoustic soot spectrometer (PASS-3), and an Aerodyne soot

Received: September 21, 2017
Revised: October 14, 2017
Accepted: October 16, 2017
Published: October 16, 2017

DOI: 10.1021/acs.estlett.7b00418
Environ. Sci. Technol. Lett. XXXX, XXX, XXX−XXX

particle−aerosol mass spectrometer (SP-AMS) were used to characterize the physicochemical properties of soot and to measure their optical properties.[11−14] However, these measurements could not provide accurate morphology of soot aggregates for the modeling study. Many numerical optical models such as the Rayleigh−Debye−Gans (RDG) approximation,[15] the T-Matrix,[16,17] and discrete dipole approximation (DDA)[18] can be used to calculate the optical properties of soot aggregates.[10,19−21] Except for the RDG model, other numerical models require the morphology of soot aggregates, which can be generated numerically using the fractal dimension (D_f). Among the available algorithms for generating fractal aggregates, the tunable method[22] is preferred because of its ability to generate aggregates of a prescribed D_f, which is the most important morphological parameter of fractal aggregates. Adachi et al.[23] used electron tomography in transmission electron microscopy (TEM) to calculate the D_f of individual soot particles. The method requires a sophisticated system of TEM coupled with tomography, which is not commonly available. Xiong and Friedlander[24] calculated the D_f of individual soot particles by drawing circles around the primary particles and then determining the size and position of the primary particles in the TEM image using scaling laws.[25,26] The method is inefficient for obtaining the D_f of hundreds of soot particles, because it requires 10−30 min for each soot aggregate. Later, an approach for image characterization of soot aggregates was proposed by Brasil et al.[27] and Oh and Sorensen.[28] The method can conveniently derive various parameters of individual soot particles in the scaling law and yield a D_f to represent their ensemble morphology. Recently, China et al.[29] successfully used this method to calculate the D_f of soot particles freshly emitted by wildfire. However, there are only quite few available reports about the D_f of ambient soot particles; their D_f values are very important for understanding their optical properties in different environments.

In this study, we report a detailed analysis of a large number of soot particles collected at tunnel, urban, mountaintop, and background sites in polluted air in the North China Plain (NCP). At each site, soot particles are classified into three types on the basis of their mixing states and morphology, and then their corresponding D_f values are calculated and compared systematically for the first time. We use a method combining TEM analysis and numerical calculation to obtain a D_f to represent the ensemble morphology of soot aggregates. Finally, we discuss their morphological and mixing properties and the implications of these properties for aging.

2. MATERIALS AND METHODS

2.1. Aerosol Sampling. The NCP was covered by the regional haze layer during the sampling period, so we defined our samples as being from the continental polluted air. Aerosol samples were collected at four sampling sites in the NCP, a tunnel site, an urban site, a mountaintop site, and a background site (Figure S1), where the relative humidities (RHs) were ~52, ~16, ~64, and ~56%, respectively. The RHs at the four sampling sites were <65% during the sampling period, indicating that the hazes were mainly dry. The Kaiyuan tunnel site is a busy highway that enters Jinan City. The urban site in Jinan City is a typical downtown site with high levels of vehicle and residential emissions. Mountain Tai (1534 m above sea level) is the tallest mountain in the NCP. The aerosol particles collected at the mountaintop site reflect the regional transport of aerosol particles in the NCP.[30] The background Changdao Island in the Bohai Sea is a downwind site of Shandong Province and the Jing-Jin-Ji area (i.e., Beijing, Tianjin, and Hebei Province) during the winter (Figure S1). Aerosol samples were simultaneously collected at the urban, mountaintop, and background sites from December 13 to 23, 2014. At the tunnel site, aerosol samples were collected on November 8, 2016. A total of 779 soot particles from 31 samples were analyzed to determine their size and elemental composition using TEM and energy-dispersive X-ray spectroscopy (EDS). We note that the distribution of aerosol particles on TEM grids was not uniform. Therefore, we chose three or four areas from the center and periphery of each grid to ensure that the analyzed particles were representative. Once the internally mixed soot particles are under the strong electron beam (Figure S2), they can easily damage the sulfates and nitrates but do not change the morphology of soot aggregates. This microscopic analysis is explained in the Supporting Information.

2.2. Morphology Analysis of Soot Particles. The fractal dimension of soot particles can be characterized using the scaling law:[25]

$$N = k_g\left(\frac{2R_g}{d_p}\right)^{D_f} \tag{1}$$

where N is the total number of monomers in each aggregate, R_g is the radius of gyration of the soot aggregate, d_p is the monomer diameter, k_g is the fractal prefactor, and D_f is the mass fractal dimension. Note that the D_f in this study is the mass fractal dimension of soot aggregates that excludes the coating. In this study, D_f and k_g are estimated from a power law fit of a scatter plot of N versus the values of $2R_g/d_p$.

N can also be scaled with the aggregate projected area in the following power law relationship:

$$N = k_a\left(\frac{A_a}{A_p}\right)^{\alpha} \tag{2}$$

$$\delta = \frac{2a}{l} \tag{3}$$

where A_a is the projected area of the soot aggregate, A_p is the mean projected area of the monomer, k_a is a constant, and α is an empirical projected area exponent. The exact values of k_a and α depend on the overlap parameter (δ),[28] which can be calculated using eq 3, with a being the monomer radius and l the lattice spacing in TEM images. The number of monomers (N) can then be calculated using eq 2.[28]

Parameters d_p and R_g are also required to determine D_f. While d_p can be obtained directly from analysis of TEM images, estimation of the actual radius of gyration (R_g) is complicated. Here we used the following simple correlation

$$L_{max}/(2R_g) = 1.50 \pm 0.05 \tag{4}$$

to calculate R_g,[27] where L_{max} is the maximum length of the soot aggregate obtained from TEM images.

3. RESULTS AND DISCUSSION

3.1. Morphology and Mixing State of Soot Particles. Fresh soot particles are normally chain-like aggregates. Once soot particles mix with other aerosol components in the air, the aging process can rearrange the structure of the inner soot aggregates.[31] On the basis of their morphology and the visual estimation of coating on soot particles in TEM images, we

DOI: 10.1021/acs.estlett.7b00418
Environ. Sci. Technol. Lett. XXXX, XXX, XXX−XXX

classified them into three types: bare-like, partly coated, and embedded. Bare-like soot particles in TEM images display clear monomers without any visible coating on their surface (Figure 1a-1−c-1). Partly coated soot particles mean that individual

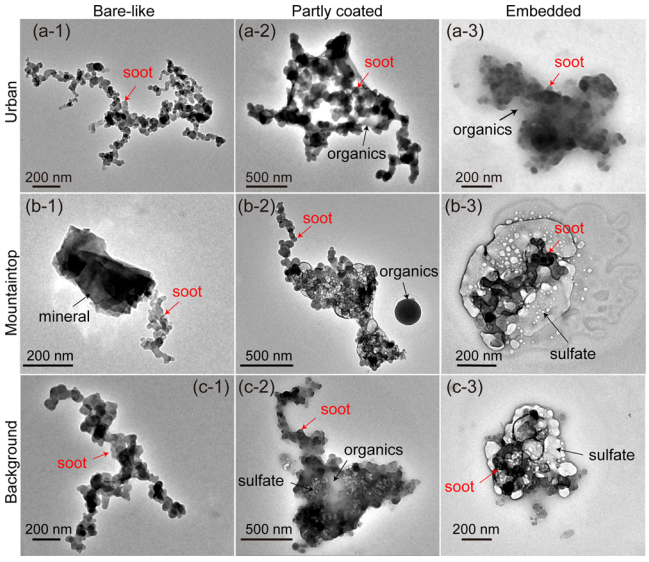

Figure 1. TEM images of individual soot particles collected at the urban site (a-1−a-3), the mountaintop site (b-1−b-3), and the background site (c-1−c-3). Soot particles are classified into three types: bare-like (a-1−c-1), partly coated (a-2−c-2), and embedded (a-3−c-3).

soot particles are partly coated by other aerosol components (Figure 1a-2−c-2). Embedded soot particles refer to individual soot particles that are heavily coated or are entirely embedded within other aerosol components (Figure 1a-3−c-3). Figure 1 shows the three types of soot particles collected at the urban, mountaintop, and background sampling sites. Bare-like soot particles are dominant in the tunnel samples, because vehicles emit large amounts of fresh soot particles (Figure S3). Similar results have been found near freeways.[32] On the basis of their different mixing structures, embedded soot particles are normally considered to be more aged than the partly coated soot particles.[33] We also calculated the coating/soot core area ratios for internally mixed soot particles. Figure S4 shows partly coated soot particles mostly have ratios of <1, indicating thinner coatings. In contrast, embedded soot particles have larger ratios, some of which are more than 20 times larger. These results are consistent with our classification.

Figure 2 shows the fractions of three types of soot particles in different atmospheric environments. The result shows that the bare-like soot particles accounted for 64% of all particles in tunnel air but only 1−25% in urban polluted air (Figure 2). Wang et al.[34] also found a fairly small fraction (31.2%) of externally mixed soot particles in urban Xi'an City of China through a single-particle soot photometer (SP2). As a result, the polluted air likely accelerated the transformation from bare-like to partly coated or embedded soot particles.[33] It should be noted that bare-like soot particles accounted for 25% at the urban site and 21% at the background site but the level of embedded soot particles significantly increased from 12 to 39% (Figure 2). These results indicate that the polluted air masses from the Jing-Jin-Ji area and Shandong Province (Figure S1) brought a large number of aged soot particles into the downwind background air. In addition, the fraction of

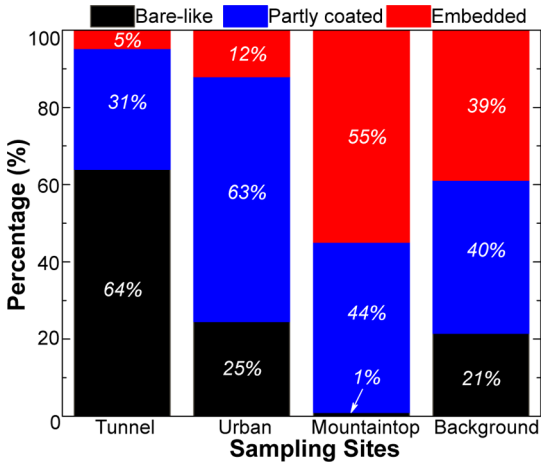

Figure 2. Percentages of bare-like, partly coated, and embedded soot particles collected at four sampling sites. In total, 147, 216, 295, and 121 soot particles were analyzed from the samples collected at the tunnel, urban, mountaintop, and background sites, respectively.

embedded soot particles at the mountaintop site is largest at 55% and the fraction of bare-like soot is lowest at 1% among the three sampling sites. China et al.[35] found that most soot particles from North America become internally mixed at the summit caldera of the Pico Volcano. Therefore, soot particles that are emitted mostly at ground level but transported into the upper atmospheric layers could undergo intense aging processes during their transport. The RH is a critical factor for enhancing heterogeneous reactions of acidic gases on a particle surface because secondary aerosols can deliquesce at approximately 60−80% RH and form liquid phases.[36] During the sampling period, there was a higher RH of ∼64% in the upper air than the RH of 16−55% on the ground. Indeed, many embedded soot particles on the mountaintop left a water rim around the sulfate coating after drying on the substrate (Figure 1b-3), which indicates that secondary aerosol components existed in the liquid phase in the air.[33] We conclude that soot particles likely underwent more complicated aging processes because the RH of the upper layers was higher than that of the polluted ground sites.

3.2. Quantifying the Shapes of Soot Particles. It is widely acknowledged that the D_f of soot particles reflects their combustion conditions and aging processes.[23] Compact soot particles often have D_f values larger than those of lacy aggregates.[37] Here we calculated the D_f values of soot particles collected at the four sampling sites (Figure 3). The D_f of bare-like soot particles at different sampling sites was very close, at ∼1.82 (Figure 3a,b,d). Bare-like soot particles have the smallest D_f followed by partly coated and embedded soot particles (Figure 3), suggesting that bare-like soot particles were more lacy than the partly coated and embedded types. The D_f of partly coated soot particles tends to be ∼1.87, smaller than the range of 1.90−2.16 of embedded soot particles (Figure 3). Similarly, China et al.[29] found the same properties (i.e., bare-like < partly coated < embedded) of D_f of the three types of soot particles emitted by wildfires. Peng et al.[38] also found that the morphology of soot particles was modified heavily during aging processes. For the background soot particles, D_f ranges between 1.83 and 2.16, with a medium of 2.00 (Figure 3d). In contrast, the D_f of the urban soot particles is lower, between 1.83 and 1.90. We multiplied the number fraction of each type of soot by their corresponding D_f to calculate the statistical

DOI: 10.1021/acs.estlett.7b00418
Environ. Sci. Technol. Lett. XXXX, XXX, XXX−XXX

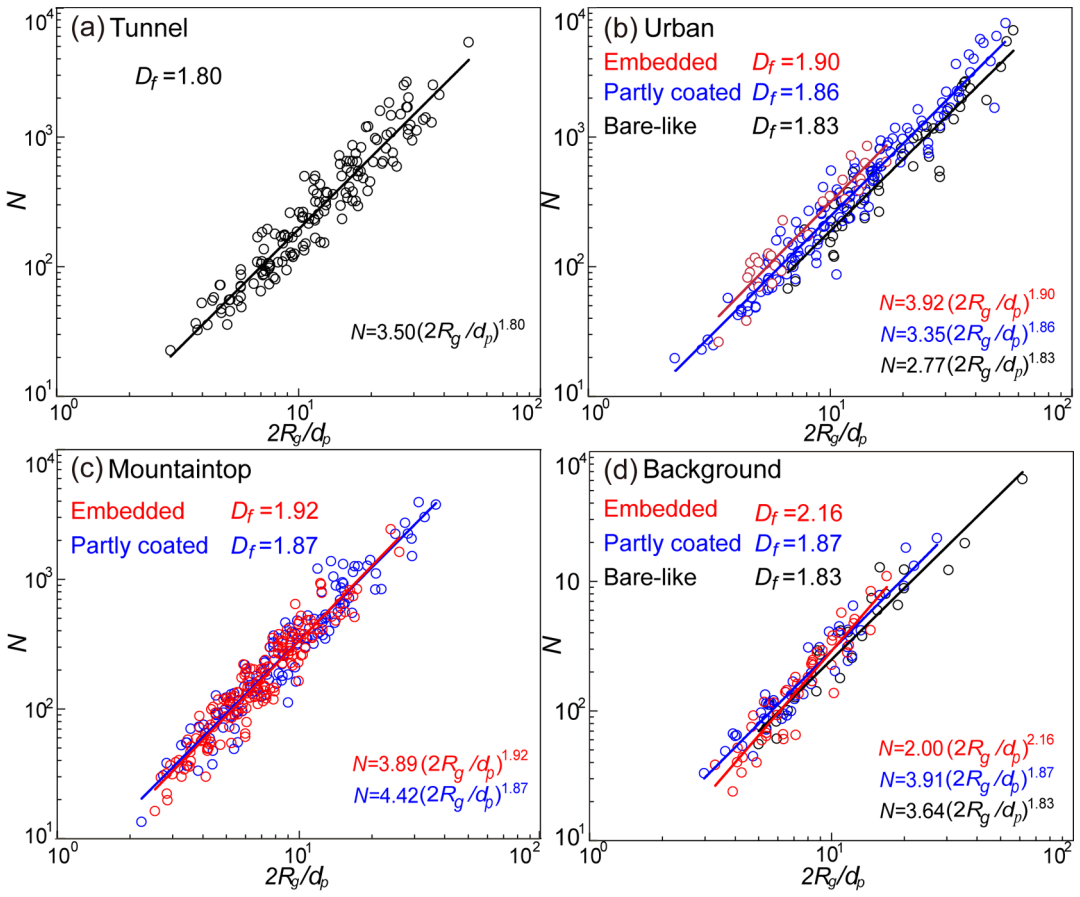

Figure 3. Fractal dimensions of different types of soot collected at the (a) tunnel, (b) urban, (c) mountaintop, and (d) background sites. For each site, the lines and circles represent bare-like (black), partly coated (blue), and embedded (red) soot particles.

weighting of D_f. The statistical weightings of D_f values of the urban, mountaintop, and background site are 1.87, 1.90, and 1.97, respectively, which yield an average of 1.91.

The convexity (CV), roundness (RN), and D_f of the three types of soot particles at the four sampling sites are listed in Table S1. The CV and RN distributions of the three types of soot particles at the same sampling site (Figure S5) clearly prove their D_f values change (Figure 3). The CV and RN of bare-like soot particles are the smallest, followed by those of partly coated and embedded soot particles at the four sampling sites. We therefore conclude that the larger CV and larger RN represent more compactness for aged soot particles, consistent with the study of China et al.[29]

We found that the D_f of fresh soot particles remained at a consistent value (~1.82) at different sampling sites in the polluted air (Figure 3), although fresh soot particles display a slightly different D_f because of their different sources and combustion conditions.[39] Many researchers obtained the D_f of soot particles of the primary sources, such as the D_f from biomass burning in the range of 1.67−1.83,[40] the D_f from vehicle emissions in the range of 1.52−1.94,[32] and the D_f from diesel in the range of 1.6−1.9.[41] The D_f of soot particles becomes larger when soot aggregates are coated by other components during atmospheric processes.[42] This indicates that soot particles likely collapse during the coating processes. In addition, the wide range of D_f of soot particles in the background air is expected because they originate from multiple sources, such as industries, residential heating, and transportation,[30] and have undergone different atmospheric aging processes with different durations.[23] In addition, the D_f values of embedded soot particles in the range of 1.90−2.16 in this study are much lower than the range of 2.3−2.6 reported in some previous studies.[21,23,43] Adachi et al.[21,23] used a cube-counting method to calculate the D_f of soot particles. In most cases, the images of fractal aggregates cannot be decomposed at all scales into an integer number of square boxes using this method,[44] which may lead to a larger D_f. In the study by Bambha et al.,[43] the smaller monomer diameter may cause less structural compaction.[45] In addition, the coating material that condensed at a low humidity often causes no restructuring; on the other hand, the coating liquefies at a higher humidity, and restructuring occurs promptly.[46] In a word, these differences could be attributed to data processing methods, aging environments, and soot aggregate properties.

Using the scaling law method, the previous studies reported D_f values in the range of 1.52−1.94 for soot particles at the road side[32] and D_f values of >2 for soot particles at a remote marine troposphere site.[35] Here we systematically studied the D_f of ambient soot particles collected at three representative polluted sites. These data are crucial for assessing the accurate shape of soot particles in the dry continental air.

4. ATMOSPHERIC IMPLICATIONS

Previous studies reported that the fractal dimensions (D_f) of fresh soot particles from vehicles, biomass, diesel, and wildfire emissions are around 1.73,[32] 1.75,[40] 1.75,[41] and 1.89,[29] respectively, which are close to the range of 1.80−1.83 (D_f) of the bare-like soot particles obtained in this study (Figure 3).

DOI: 10.1021/acs.estlett.7b00418
Environ. Sci. Technol. Lett. XXXX, XXX, XXX−XXX

This is true because fresh soot particles are generally formed via a cluster-dilute aggregation mechanism in a small-scale burning regime.[39,47] These fresh soot particles are hydrophobic before they are affected by secondary aerosols and condensable vapors in the atmosphere.[48] Therefore, fresh soot particles can hardly collapse, and their structures remain largely unchanged. In contrast, once soot particles interact with secondary organic and inorganic aerosols and water vapor during long-range transport, they became more compact as evidenced by the larger D_f in mountaintop and background air (Figure 3). TEM images further show that the morphology of soot particles not only became more compact from vehicular emission to background air (Figure 1) but also possibly underwent reconstruction under the influence of water vapor.[5,49] Therefore, these hygroscopic secondary aerosols heavily caused morphological changes of soot particles in the atmosphere.

In this study, the D_f values of soot particles were found to vary from 1.80 to 2.16 (Figure 3d) for different mixing structures, which indicate that the mixing structures of soot particles can represent their degree of aging.[31,33] At present, many studies set the D_f to ∼1.8 to simulate the complex structure of soot particles and to further calculate their optical properties.[10,50−52] However, some studies have suggested that the highly compact soot particles have optical properties substantially different from those of the lacy ones.[20,53,54] In particular, the mass-specific scattering cross sections (MSC) of soot particles decrease in the following order: $D_f = 2.1 > D_f = 1.78 > D_f = 1.4$.[20] Therefore, it is essential to select suitable D_f values to construct accurate optical models of soot particles. Our results show that the statistical weighting of D_f of soot samples collected at the urban, mountaintop, and background sites has an average value of 1.91, suggesting that the D_f of 1.91 could be more representative of ambient soot particles in continental polluted air. In particular, the D_f of 1.91 can well represent soot particles in dry (<65% RH), winter polluted air in North China Plain. Further studies are required to quantify the D_f of soot particles in different atmospheric environments, such as in humid, troposphere, and strongly photochemical air, because they all can accelerate the aging of soot in the atmosphere.[5,34]

■ ASSOCIATED CONTENT

Supporting Information

The Supporting Information is available free of charge on the ACS Publications website at DOI: 10.1021/acs.estlett.7b00418.

Specific microscopic analysis, related geometric parameters of soot particles, and some supplementary tables and figures (PDF)

■ AUTHOR INFORMATION

Corresponding Author

*E-mail: liweijun@zju.edu.cn. Phone: +86-57187952453.

ORCID

Yuanyuan Wang: 0000-0003-4190-6418
Cenlin He: 0000-0002-7367-2815
Weijun Li: 0000-0003-4887-4260

Notes

The authors declare no competing financial interest.

■ ACKNOWLEDGMENTS

The authors thank Peter Hyde for his editorial comments. This work was funded by the National Natural Science Foundation of China (41622504 and 41575116) and the Hundred Talents Program in Zhejiang University. Z.S. is supported by the Natural Environment Research Council (NE/N007190/1).

■ REFERENCES

(1) Bond, T. C.; Streets, D. G.; Yarber, K. F.; Nelson, S. M.; Woo, J. H.; Klimont, Z. A technology-based global inventory of black and organic carbon emissions from combustion. *J. Geophys. Res.* **2004**, *109*, 1149−1165.

(2) Ramanathan, V.; Carmichael, G. Global and regional climate changes due to black carbon. *Nat. Geosci.* **2008**, *1*, 221−227.

(3) Bond, T. C.; Doherty, S. J.; Fahey, D. W.; Forster, P. M.; Berntsen, T.; Deangelo, B. J.; Flanner, M. G.; Ghan, S.; Kärcher, B.; Koch, D.; et al. Bounding the role of black carbon in the climate system: A scientific assessment. *J. Geophys. Res.: Atmos.* **2013**, *118*, 5380−5552.

(4) Adler, G.; Riziq, A. A.; Erlick, C.; Rudich, Y. Effect of intrinsic organic carbon on the optical properties of fresh diesel soot. *Proc. Natl. Acad. Sci. U. S. A.* **2010**, *107*, 6699−6704.

(5) Zhang, R.; Khalizov, A. F.; Pagels, J.; Zhang, D.; Xue, H.; McMurry, P. H. Variability in morphology, hygroscopicity, and optical properties of soot aerosols during atmospheric processing. *Proc. Natl. Acad. Sci. U. S. A.* **2008**, *105*, 10291−10296.

(6) Zhou, C.; Zhang, H.; Zhao, S.; Li, J. Simulated effects of internal mixing of anthropogenic aerosols on the aerosol−radiation interaction and global temperature. *International Journal of Climatology* **2017**, *37*, 972−986.

(7) Jacobson, M. Z. Strong radiative heating due to the mixing state of black carbon in atmospheric aerosols. *Nature* **2001**, *409*, 695−697.

(8) Cappa, C. D.; Onasch, T. B.; Massoli, P.; Worsnop, D. R.; Bates, T. S.; Cross, E. S.; Davidovits, P.; Hakala, J.; Hayden, K. L.; Jobson, B. T.; Kolesar, K. R.; Lack, D. A.; Lerner, B. M.; Li, S.-M.; Mellon, D.; Nuaaman, I.; Olfert, J. S.; Petäjä, T.; Quinn, P. K.; Song, C.; Subramanian, R.; Williams, E. J.; Zaveri, R. A. Radiative Absorption Enhancements Due to the Mixing State of Atmospheric Black Carbon. *Science* **2012**, *337*, 1078−1081.

(9) Liu, D.; Whitehead, J.; Alfarra, M. R.; Reyes-Villegas, E.; Spracklen, D. V.; Reddington, C. L.; Kong, S.; Williams, P. I.; Ting, Y.-C.; Haslett, S.; Taylor, J. W.; Flynn, M. J.; Morgan, W. T.; McFiggans, G.; Coe, H.; Allan, J. D. Black-carbon absorption enhancement in the atmosphere determined by particle mixing state. *Nat. Geosci.* **2017**, *10*, 184−188.

(10) Scarnato, B. V.; Vahidinia, S.; Richard, D. T.; Kirchstetter, T. W. Effects of internal mixing and aggregate morphology on optical properties of black carbon using a discrete dipole approximation model. *Atmos. Chem. Phys.* **2013**, *13*, 5089−5101.

(11) Wang, J.; Ge, X.; Chen, Y.; Shen, Y.; Zhang, Q.; Sun, Y.; Xu, J.; Ge, S.; Yu, H.; Chen, M. Highly time-resolved urban aerosol characteristics during springtime in Yangtze River Delta, China: insights from soot particle aerosol mass spectrometry. *Atmos. Chem. Phys.* **2016**, *16*, 9109−9127.

(12) Lan, Z.-J.; Huang, X.-F.; Yu, K.-Y.; Sun, T.-L.; Zeng, L.-W.; Hu, M. Light absorption of black carbon aerosol and its enhancement by mixing state in an urban atmosphere in South China. *Atmos. Environ.* **2013**, *69*, 118−123.

(13) Liu, S.; Aiken, A. C.; Gorkowski, K.; Dubey, M. K.; Cappa, C. D.; Williams, L. R.; Herndon, S. C.; Massoli, P.; Fortner, E. C.; Chhabra, P. S.; Brooks, W. A.; Onasch, T. B.; Jayne, J. T.; Worsnop, D. R.; China, S.; Sharma, N.; Mazzoleni, C.; Xu, L.; Ng, N. L.; Liu, D.; Allan, J. D.; Lee, J. D.; Fleming, Z. L.; Mohr, C.; Zotter, P.; Szidat, S.; Prevot, A. S. Enhanced light absorption by mixed source black and brown carbon particles in UK winter. *Nat. Commun.* **2015**, *6*, 8435.

(14) Wang, J.; Onasch, T. B.; Ge, X.; Collier, S.; Zhang, Q.; Sun, Y.; Yu, H.; Chen, M.; Prévôt, A. S. H.; Worsnop, D. R. Observation of

DOI: 10.1021/acs.estlett.7b00418
Environ. Sci. Technol. Lett. XXXX, XXX, XXX−XXX

Fullerene Soot in Eastern China. *Environ. Sci. Technol. Lett.* **2016**, *3*, 121−126.
(15) Farias, T. L.; Köylü, U.; Carvalho, M. G. Range of validity of the Rayleigh-Debye-Gans theory for optics of fractal aggregates. *Appl. Opt.* **1996**, *35*, 6560−6567.
(16) Bi, L.; Yang, P.; Kattawar, G. W.; Mishchenko, M. I. Efficient implementation of the invariant imbedding T-matrix method and the separation of variables method applied to large nonspherical inhomogeneous particles. *J. Quant. Spectrosc. Radiat. Transfer* **2013**, *116*, 169−183.
(17) Mackowski, D. W.; Mishchenko, M. I. A multiple sphere T-matrix Fortran code for use on parallel computer clusters. *J. Quant. Spectrosc. Radiat. Transfer* **2011**, *112*, 2182−2192.
(18) Draine, B. T.; Flatau, P. J. Discrete-Dipole Approximation For Scattering Calculations. *J. Opt. Soc. Am. A* **1994**, *11*, 1491−1499.
(19) Liu, C.; Yin, Y.; Hu, F.; Jin, H.; Sorensen, C. M. The Effects of Monomer Size Distribution on the Radiative Properties of Black Carbon Aggregates. *Aerosol Sci. Technol.* **2015**, *49*, 928−940.
(20) Liu, F.; Wong, C.; Snelling, D. R.; Smallwood, G. J. Investigation of Absorption and Scattering Properties of Soot Aggregates of Different Fractal Dimension at 532 nm Using RDG and GMM. *Aerosol Sci. Technol.* **2013**, *47*, 1393−1405.
(21) Adachi, K.; Chung, S. H.; Buseck, P. R. Shapes of soot aerosol particles and implications for their effects on climate. *J. Geophys. Res.* **2010**, *115*, 4447−4458.
(22) Skorupski, K.; Mroczka, J.; Wriedt, T.; Riefler, N. A fast and accurate implementation of tunable algorithms used for generation of fractal-like aggregate models. *Phys. A* **2014**, *404*, 106−117.
(23) Adachi, K.; Chung, S. H.; Friedrich, H.; Buseck, P. R. Fractal parameters of individual soot particles determined using electron tomography: Implications for optical properties. *J. Geophys. Res.* **2007**, *112*, 2156−2202.
(24) Xiong, C.; Friedlander, S. K. Morphological properties of atmospheric aerosol aggregates. *Proc. Natl. Acad. Sci. U. S. A.* **2001**, *98*, 11851−11856.
(25) Koeylue, U.; Xing, Y.; Rosner, D. E. Fractal Morphology Analysis of Combustion-Generated Aggregates Using Angular Light Scattering and Electron Microscope Images. *Langmuir* **1995**, *11*, 4848−4854.
(26) Forrest, S. R.; Witten, T. A. J., Long-range correlations in smoke-particle aggregates. *J. Phys. A: Math. Gen.* **1979**, *12*, L109−L117.
(27) Brasil, A. M.; Farias, T. L.; Carvalho, M. G. A recipe for image characterization of fractal-like aggregates. *J. Aerosol Sci.* **1999**, *30*, 1379−1389.
(28) Oh, C.; Sorensen, C. M. The Effect of Overlap between Monomers on the Determination of Fractal Cluster Morphology. *J. Colloid Interface Sci.* **1997**, *193*, 17−25.
(29) China, S.; Mazzoleni, C.; Gorkowski, K.; Aiken, A. C.; Dubey, M. K. Morphology and mixing state of individual freshly emitted wildfire carbonaceous particles. *Nat. Commun.* **2013**, *4*, 2122.
(30) Chen, S.; Xu, L.; Zhang, Y.; Chen, B.; Wang, X.; Zhang, X.; Zheng, M.; Chen, J.; Wang, W.; Sun, Y.; Fu, P.; Wang, Z.; Li, W. Direct observations of organic aerosols in common wintertime hazes in North China: insights into direct emissions from Chinese residential stoves. *Atmos. Chem. Phys.* **2017**, *17*, 1259−1270.
(31) Riemer, N.; Vogel, H.; Vogel, B. Soot aging time scales in polluted regions during day and night. *Atmos. Chem. Phys.* **2004**, *4*, 1885−1893.
(32) China, S.; Salvadori, N.; Mazzoleni, C. Effect of traffic and driving characteristics on morphology of atmospheric soot particles at freeway on-ramps. *Environ. Sci. Technol.* **2014**, *48*, 3128−3135.
(33) Li, W.; Sun, J.; Xu, L.; Shi, Z.; Riemer, N.; Sun, Y.; Fu, P.; Zhang, J.; Lin, Y.; Wang, X.; Shao, L.; Chen, J.; Zhang, X.; Wang, Z.; Wang, W. A conceptual framework for mixing structures in individual aerosol particles. *J. Geophys. Res.: Atmos.* **2016**, *121*, 13784−13798.
(34) Wang, Q.; Huang, R. J.; Cao, J.; Han, Y.; Wang, G.; Li, G.; Wang, Y.; Dai, W.; Zhang, R.; Zhou, Y. Mixing State of Black Carbon Aerosol in a Heavily Polluted Urban Area of China: Implications for Light Absorption Enhancement. *Aerosol Sci. Technol.* **2014**, *48*, 689−697.
(35) China, S.; Scarnato, B.; Owen, R. C.; Zhang, B.; Ampadu, M. T.; Kumar, S.; Dzepina, K.; Dziobak, M. P.; Fialho, P.; Perlinger, J. A.; Hueber, J.; Helmig, D.; Mazzoleni, L. R.; Mazzoleni, C. Morphology and mixing state of aged soot particles at a remote marine free troposphere site: Implications for optical properties. *Geophys. Res. Lett.* **2015**, *42*, 1243−1250.
(36) Peckhaus, A.; Grass, S.; Treuel, L.; Zellner, R. Deliquescence and efflorescence behavior of ternary inorganic/organic/water aerosol particles. *J. Phys. Chem. A* **2012**, *116*, 6199−6210.
(37) Liu, L.; Mishchenko, M. I.; Patrick Arnott, W. A study of radiative properties of fractal soot aggregates using the superposition T-matrix method. *J. Quant. Spectrosc. Radiat. Transfer* **2008**, *109*, 2656−2663.
(38) Peng, J.; Hu, M.; Guo, S.; Du, Z.; Zheng, J.; Shang, D.; Levy Zamora, M.; Zeng, L.; Shao, M.; Wu, Y. S.; Zheng, J.; Wang, Y.; Glen, C. R.; Collins, D. R.; Molina, M. J.; Zhang, R. Markedly enhanced absorption and direct radiative forcing of black carbon under polluted urban environments. *Proc. Natl. Acad. Sci. U. S. A.* **2016**, *113*, 4266−4271.
(39) Chakrabarty, R. K.; Beres, N. D.; Moosmüller, H.; China, S.; Mazzoleni, C.; Dubey, M. K.; Liu, L.; Mishchenko, M. I. Soot superaggregates from flaming wildfires and their direct radiative forcing. *Sci. Rep.* **2015**, *4*, 5508.
(40) Chakrabarty, R. K.; Moosmüller, H.; Garro, M. A.; Arnott, W. P.; Walker, J.; Susott, R. A.; Babbitt, R. E.; Wold, C. E.; Lincoln, E. N.; Hao, W. M. Emissions from the laboratory combustion of wildland fuels: Particle morphology and size. *J. Geophys. Res.* **2006**, *111*, D07204.
(41) Wentzel, M.; Gorzawski, H.; Naumann, K. H.; Saathoff, H.; Weinbruch, S. Transmission electron microscopical and aerosol dynamical characterization of soot aerosols. *J. Aerosol Sci.* **2003**, *34*, 1347−1370.
(42) Chen, C.; Fan, X.; Shaltout, T.; Qiu, C.; Ma, Y.; Goldman, A.; Khalizov, A. F. An unexpected restructuring of combustion soot aggregates by subnanometer coatings of polycyclic aromatic hydrocarbons. *Geophys. Res. Lett.* **2016**, *43*, 11080−11088.
(43) Bambha, R. P.; Dansson, M. A.; Schrader, P. E.; Michelsen, H. A. Effects of volatile coatings and coating removal mechanisms on the morphology of graphitic soot. *Carbon* **2013**, *61*, 80−96.
(44) Wozniak, M.; Onofri, F. R. A.; Barbosa, S.; Yon, J.; Mroczka, J. Comparison of methods to derive morphological parameters of multi-fractal samples of particle aggregates from TEM images. *J. Aerosol Sci.* **2012**, *47*, 12−26.
(45) Leung, K. K.; Schnitzler, E. G.; Dastanpour, R.; Rogak, S. N.; Jäger, W.; Olfert, J. S. Relationship between Coating-Induced Soot Aggregate Restructuring and Primary Particle Number. *Environ. Sci. Technol.* **2017**, *51*, 8376−8383.
(46) Leung, K. K.; Schnitzler, E. G.; Jäger, W.; Olfert, J. S. Relative Humidity Dependence of Soot Aggregate Restructuring Induced by Secondary Organic Aerosol: Effects of Water on Coating Viscosity and Surface Tension. *Environ. Sci. Technol. Lett.* **2017**, *4*, 386−390.
(47) Sorensen, C. M.; Chakrabarti, A. The sol to gel transition in irreversible particulate systems. *Soft Matter* **2011**, *7*, 2284−2296.
(48) Tritscher, T.; Jurányi, Z.; Martin, M.; Chirico, R.; Gysel, M.; Heringa, M. F.; DeCarlo, P. F.; Sierau, B.; Prévôt, A. S. H.; Weingartner, E.; Baltensperger, U. Changes of hygroscopicity and morphology during ageing of diesel soot. *Environ. Res. Lett.* **2011**, *6*, 034026.
(49) Ma, X.; Zangmeister, C. D.; Gigault, J.; Mulholland, G. W.; Zachariah, M. R. Soot aggregate restructuring during water processing. *J. Aerosol Sci.* **2013**, *66*, 209−219.
(50) Filippov, A. V.; Zurita, M.; Rosner, D. E. Fractal-like Aggregates: Relation between Morphology and Physical Properties. *J. Colloid Interface Sci.* **2000**, *229*, 261−273.
(51) Wu, Y.; Cheng, T.; Zheng, L.; Chen, H. Optical properties of the semi-external mixture composed of sulfate particle and different

DOI: 10.1021/acs.estlett.7b00418
Environ. Sci. Technol. Lett. XXXX, XXX, XXX−XXX

quantities of soot aggregates. *J. Quant. Spectrosc. Radiat. Transfer* **2016**, *179*, 139−148.
(52) Smith, A. J. A.; Grainger, R. G. Simplifying the calculation of light scattering properties for black carbon fractal aggregates. *Atmos. Chem. Phys.* **2014**, *14*, 7825−7836.
(53) Radney, J. G.; You, R.; Ma, X.; Conny, J. M.; Zachariah, M. R.; Hodges, J. T.; Zangmeister, C. D. Dependence of soot optical properties on particle morphology: measurements and model comparisons. *Environ. Sci. Technol.* **2014**, *48*, 3169−76.
(54) He, C.; Takano, Y.; Liou, K.-N.; Yang, P.; Li, Q.; Mackowski, D. W. Intercomparison of the GOS approach, superposition T-matrix method, and laboratory measurements for black carbon optical properties during aging. *J. Quant. Spectrosc. Radiat. Transfer* **2016**, *184*, 287−296.

DOI: 10.1021/acs.estlett.7b00418
Environ. Sci. Technol. Lett. XXXX, XXX, XXX−XXX